Jamming graphs: A local approach to global mechanical rigidity

Jorge H. Lopez, L. Cao, and J. M. Schwarz
Department of Physics, Syracuse University, Syracuse, New York 13244, USA
(Received 19 June 2013; published 16 December 2013)

We revisit the concept of minimal rigidity as applied to frictionless, repulsive soft sphere packings in two dimensions with the introduction of the jamming graph. Minimal rigidity is a purely combinatorial property encoded via Laman's theorem in two dimensions. It constrains the global, average coordination number of the graph, for example. However, minimal rigidity does not address the geometry of local mechanical stability. The jamming graph contains both properties of global mechanical stability at the onset of jamming and local mechanical stability. We demonstrate how jamming graphs can be constructed using local moves via the Henneberg construction such that these graphs fall under the jurisdiction of correlated percolation. We then probe how jamming graphs destabilize, or become unjammed, by deleting a bond and computing the resulting rigid cluster distribution. We also study how the system restabilizes with the addition of new contacts and how a jamming graph with extra (redundant) contacts destabilizes. The latter endeavor allows us to probe a disk packing in the rigid phase and uncover a potentially new diverging length scale associated with the random deletion of contacts as compared to the study of cut-out (or frozen-in) subsystems.

DOI: 10.1103/PhysRevE.88.062130 PACS number(s): 64.60.De, 46.65.+g, 02.10.Ox

I. INTRODUCTION

A model system for understanding the onset of rigidity in disordered particle packing is a d-dimensional collection of frictionless, repulsive soft spheres at zero temperature [1–5]. At small packing densities, minimal energy configurations are those with no contacts between particles. As the packing density is increased, the contact geometry abruptly changes from nonexistent to one where the average coordination number equals $2d$ [2]. Moreover, the local coordination number for each particle must be at least $d+1$ in accordance with the Hilbert stability condition, or local mechanical stability [6]. As the packing density is increased even further, the average coordination number exceeds $2d$ with each particle still obeying the Hilbert stability criterion. See Fig. 1 for an example of a disordered particle packing for a bidisperse system in this regime.

The abrupt jump in contact geometry indeed has the flavor of a phase transition even though no symmetries in the positions of the particles are broken [2–4]. Continuous transitions are typically accompanied by at least one diverging length scale at the transition, such as connectivity percolation [7]. Discontinuous transitions, however, are not typically characterized by any diverging length scales. And yet, Wyart and collaborators [8,9] identified a diverging length scale in the disordered solid phase, denoted as l^*, such that the combination of the discontinuous jump in the average contact number and the diverging length scale suggests a more exotic mixed transition, such as that found in k-core percolation [10].

This length scale, l^*, can be determined by finding a cut-out subsystem of some length below which there exists extended zero-energy modes within the subsystem and above which there does not. At the transition, extended zero-energy modes proliferate due to the absence of redundant contacts, and l^* is of order the system size. As the system solidifies further with added redundant contacts, l^* decreases since such contacts make it less likely for zero-energy modes to extend across the subsystem. In practice, this length scale l^* is inferred from numerical measurements of the frequency at which the density of states deviates from the plateau region emerging at low frequencies. Very recently, however, a new construction of l^* via rigid clusters resulted in a direct numerical measurement [11]. Another length scale associated with subsystems with fixed boundaries (as opposed to cut or free boundaries) has been recently identified and scales similarly with l^* [12–14], though corrections to scaling are discussed [12,13].

While the focus on identifying a diverging length scale has been on the competition between bulk and boundary effects when cutting out a subsystem and probing for extended zero-energy modes, little work has been done to search for a length scale associated with a change in the zero-energy mode structure in response to the breaking of one or several

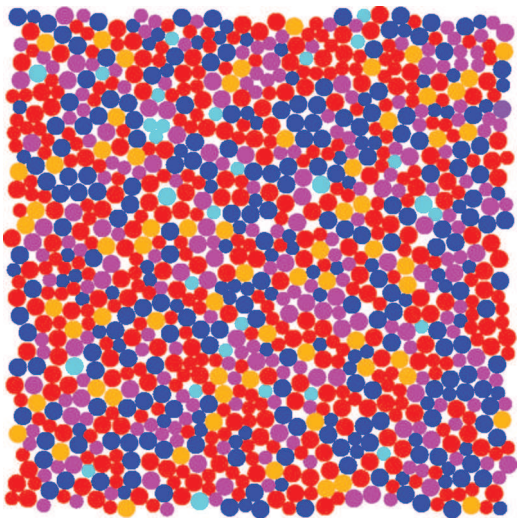

FIG. 1. (Color online) A jammed, bidisperse particle packing with $N = 1024$ and packing fraction $\phi = 0.841$. The colors denote the local coordination number, z, with light blue (very light grey) denoting $z = 0$, magenta (medium gray) denoting $z = 3$, red (dark grey) denoting $z = 4$, blue (very dark grey) denoting $z = 5$, orange (light gray) depicting $z = 6$, and purple (dark medium gray) denoting $z = 7$.

contacts, for example. After all, when searching for diverging length scales in systems undergoing phase transitions, one typically perturbs the system and computes the length scale over which the system responds to that perturbation. And while prior focus on cut-out subsystems has certainly proved useful, we ask what can be learned from removing one or two contacts and looking for a length scale over which the perturbation affects the mode structure. Point perturbations have been performed when investigating the force network of the particle packing above jamming [15,16] and on phonon modes in floppy networks, i.e., below jamming [17]. Here, we explore random bond deletion effects on the structure of zero-energy modes via the study of rigid clusters, and we ask the following: Does some diverging length scale fall out of such computations? If so, is this length scale similar to l^*?

To begin to answer these questions, we first present a way to build the contact geometry of polydisperse, frictionless, repulsive soft disks in two dimensions at the onset of rigidity. We do so with vertices representing particles and bonds representing contacts between particles. After all, at the transition there are no forces, i.e., the particles are in contact but not overlapping, so one does not necessarily need to rely on forces explicitly to generate the packing. This jamming graph algorithm uses spatially local rules to generate the contact geometry in two dimensions—local rules that encode the global rule of minimal rigidity. Interestingly, the percolation transition, with its local rules, can be described by a field theory [18]. If the abrupt changes in contact geometry in the frictionless, repulsive soft sphere system can also be characterized by local rules, can such a system be described by a field theory? After introducing our algorithm, we then perturb the contact geometry of the jamming graph and study the resulting rigid cluster distributions.

The study of rigid clusters has its roots in rigidity percolation [19–21]. In rigidity percolation, one demands that the cluster spanning a system of randomly diluted bonds on a lattice be rigid in the sense that if each bond were associated with, for example, a spring, then there would be a finite energy cost to deforming the cluster. In two dimensions, numerical studies suggest that the onset of rigidity is a continuous phase transition [22–24]. Rigidity percolation differs from jamming in that jamming occurs in a particulate system, where particles can come in and out of contact, i.e., the connectivity is not fixed. Rigidity percolation also differs from both jamming and the jamming graph in that there are local constraints on the geometry to take into account local mechanical stability in the presence of purely repulsive forces.

The paper is organized as follows. Section II discusses the local and global properties of the contact geometry of frictionless, repulsive soft spheres. Section III presents the algorithm for building a jamming graph, Sec. IV addresses perturbations of the jamming graph, and Sec. V discusses the implications of our results.

II. CONTACT GEOMETRY OF FRICTIONLESS, REPULSIVE SOFT SPHERES AT THE ONSET OF RIGIDITY

The initial link between contact geometry and the onset of rigidity in mechanical networks with fixed connectivity is due to Maxwell via the Maxwell constraint counting condition [25]. This is a necessary (but not sufficient) condition for mechanical rigidity. It does so by counting the number of zero-energy (floppy) modes in the network, N_f, which depends on the number of independent constraints, N_c, and the local degrees of freedom for each particle. For mechanical networks with particles interacting via central forces,

$$N_f = Nd - N_c, \tag{1}$$

where N is the number of particles in the network. The onset of rigidity, or minimal rigidity, occurs when N_f equals the number of global degrees of freedom of the network, N_g. When $N_f = N_g$, the network is minimally rigid and the removal of just one edge in the network makes it flexible. In mean field, one can replace N_c with $\langle z \rangle \frac{N}{2}$, where $\langle z \rangle$ is the average coordination number such that the minimally rigid condition in the large-N limit becomes $\langle z \rangle = 2d$, i.e., isostaticity. Numerical simulations indicate that the onset of mechanical rigidity for soft repulsive, frictionless spheres corresponds to the isostatic condition even though the connectivity of the system is not fixed [2].

In two dimensions, one can extend the above necessary condition for minimal rigidity in central-force fixed connectivity networks, such as the ones studied in rigidity percolation, to a necessary and sufficient condition using Laman's theorem [26]: A network with N vertices is generically minimally rigid in two dimensions if and only if it has $2N - 3$ bonds and no subgraph of n vertices has more than $2n - 3$ bonds. Laman's theorem is global (or spatially nonlocal) in the sense that it involves all possible subgraphs. However, we will present a construction of the Laman graph implemented via spatially local rules involving both the addition and deletion of bonds developed earlier by Henneberg [27]. Such an algorithm falls under the jurisdiction of correlated percolation where there are constraints on the occupation of bonds as the graph is constructed. Note that for Laman's theorem, $N_g = 3$. Moreover, a recent generalization of Laman's theorem to $kN - N_g$ extends the concept of minimal rigidity [28].

Fixed connectivity central-force networks from rigidity percolation and soft, repulsive disks differ from each other in the following two ways. In the particulate system, the contacts are not fixed. These contacts break or rearrange as the system minimizes its energy or responds to perturbations. Additionally, there are only repulsive forces in the particulate system in contrast to central-force networks, which are typically spring networks exhibiting both attractive and repulsive forces. Do these differences have any implications for characterizing the contact geometry of the particulate system at the onset of rigidity, or jamming? Indeed, they do. At the transition, in addition to the system being minimally rigid, each particle must be locally mechanical stable in the presence of purely repulsive forces. Otherwise, an infinitesimal perturbation can break a contact and the system becomes flexible.

What does local mechanical stability mean in terms of constraints on the contact geometry? In two dimensions, a particle must have at least three contacts, and those contacts must be organized in such a way that the particle cannot escape its local environment via a perturbation. More precisely, any particle should have at least three neighbors, i.e., it is $3-$ core, and the particle should be inside a triangle determined by at

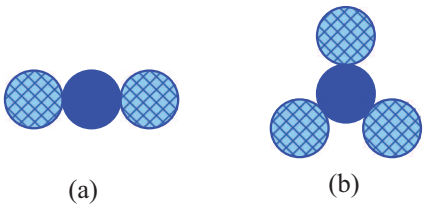

FIG. 2. (Color online) (a) The center particle is not mechanically stable (for the other two particles fixed). (b) The center particle is mechanically stable.

least three of its neighbors [6]. This local geometric condition is known as the Hilbert stability condition and is illustrated in Fig. 2. If this local condition is not obeyed, then the entire packing can become unstable due to an infinitesimal, local perturbation.

Therefore, just as Alexander [6] argued that the concept of geometrical rigidity for spring networks, when extended to particle networks, needs to incorporate the breaking of contacts, the rigidity transition for frictionless, repulsive soft disks in two dimensions is characterized by a spanning, planar graph obeying both the Laman condition *and* the principle of local mechanical stability (Hilbert stability). We call this graph a "jamming graph." The vertices in the graph represent the particles, and since the bonds represent particle contacts, the graph must be planar.

We would like to understand how such graphs obeying both global and local rules of mechanical stability are constructed in practice. It turns out that we will be able to do so using an algorithm with spatially local moves. This is because one can build a Laman graph via an algorithm called the Henneberg construction [27]. The algorithm will be presented in the following section. Therefore, we now explore the notion of minimal rigidity in particle packings in two dimensions, where the connectivity is not fixed and the forces exerted above jamming are purely repulsive, by imposing *both* types of mechanical stability.

III. ALGORITHM FOR BUILDING JAMMING GRAPHS

A. Henneberg construction

Let us review the Henneberg construction [27]. For constructing a Laman graph, we begin with a triangle and then add a vertex and connect it to prior vertices using the Henneberg steps type I and type II defined as follows:

(i) Type I step: Add a vertex and join it to two prior vertices via two new bonds.

(ii) Type II step: Add a vertex and join it to three prior vertices with at least one bond in between the three bonds. Remove a prior bond between the three connecting prior vertices.

See Fig. 3 for an illustration of the Henneberg construction.

A graph constructed using the Henneberg construction is Laman [26]. We can see this via induction. Suppose the current graph G is Laman with N vertices and $2N-3$ bonds. For the type I step: Add vertex x. Graph G now contains $N+1$ vertices and $2N-3+2=2(N+1)-3$ bonds. For any subgraph with n vertices, if it does not include x, by the induction hypothesis, there are at most $2n-3$ bonds. If the subgraph includes x, for the other $n-1$ vertices, there are at most $2(n-1)-3$ bonds between them, so in total there are at most $2(n-1)-3+2=2n-3$ bonds.

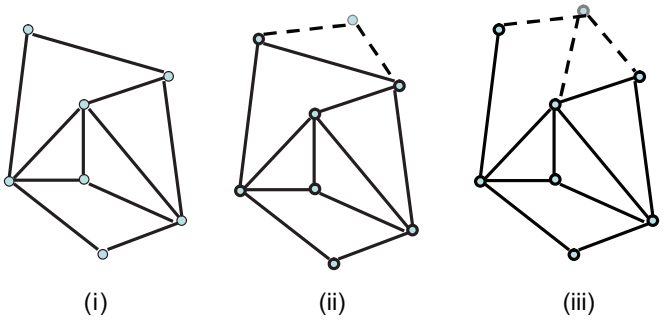

FIG. 3. (Color online) (i) Graph before the Henneberg step. (ii) The type I step with the new bonds denoted with dashed lines. (iii) Type II step.

For the type II step: Add vertex x and connect it to a, b, c. Graph G now contains $N+1$ vertices and $2N-3+3-1=2(N+1)-3$ bonds. For any subgraph with n vertices, if it does not include x, by the induction hypothesis, there are at most $2n-3$ bonds. If any subgraph includes x, for the other $n-1$ nodes, there are at most (i) $2(n-1)-3$ bonds, if not all of a, b, c are included, and (ii) $2(n-1)-4$ bonds, if a, b, c are all included.

In case (i), there are at most $2(n-1)-3+2=2n-3$ bonds. In case (ii), there are at most $2(n-1)-4+3=2n-3$ bonds. Thus, the Laman condition is satisfied. One can also show that every Laman graph can be decomposed into a Henneberg construction.

The Henneberg construction (and the corresponding Laman theorem) is purely combinatorial. It only deals with adjacency and not where the neighbors are located spatially. Because bonds in the jamming graph represent contacts between particles, we impose a planarity, or no-crossing condition, on the bonds. Moreover, if $N_g=2$, as opposed to $N_g=3$, the above Henneberg construction is unchanged.

B. Hilbert stability

We also invoke the local Hilbert stability condition for two-dimensional packings, which states that any vertex should have at least three neighbors, i.e., it is $3-$core, and the vertex should be inside a triangle determined by at least three of its neighbors [6]. To determine whether or not a vertex is enclosed in a triangle by at least three of its neighbors, we implement an algorithm based on the Jordan curve theorem [29]. It consists of drawing a horizontal line from the vertex and determining how many crossings the horizontal line makes with the enclosed triangle. If there are an odd number of crossings, then the vertex is inside the polygon as illustrated in Fig. 4.

C. Pseudocode

Graphs built by using Henneberg type II steps have typically more counterbalanced vertices since the new vertex has more neighbors in comparison to type I. So we build a jamming graph implementing Henneberg type II steps only. The graph must be planar and we implement periodic boundary

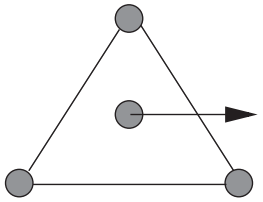

FIG. 4. Illustration for checking if a particle is enclosed by a triangle.

conditions on a square of length unity. We then enforce the Hilbert stability condition on each vertex. Here is the pseudocode of our algorithm.

(i) Create a triangle. The length of the bonds is chosen randomly from the uniform distribution on the interval $[r_{\min}, r_{\max}]$, where $r_{\min} < r_{\max} < 0.5$. The triangle is a minimally rigid $k = 3$, $N_g = 3$ structure.

(ii) Create a new vertex with random coordinates with the constraint that no vertex be less than a distance $r_{\min}$ or greater than a distance $r_{\max}$ from any other vertex and establish its neighbors according to the type II Henneberg step. This creation is successful if the new bonds are not overlapping any of the surviving prior bonds (keeping in mind that a type II Henneberg move implies the deletion of a prior bond).

(iii) Repeat the above step $N - 4$ times to create a planar Laman graph with N vertices.

(iv) Check for those vertices that are not counterbalanced.

(v) For each vertex that is not yet counterbalanced, impose the following set of strategies to enforce counterbalance. The strategies differ depending on whether an uncounterbalanced vertex has at least two neighbors or at least three.

(vi) *Counterbalance strategies for a vertex with at least three neighbors*: Suppose uncounterbalanced vertex p has neighbors n_1, n_2, and n_3, as shown in Fig. 5. If p has more than three neighbors, we apply the following strategy to each set of the three different neighbors of p. Choose n_2 such that $\overrightarrow{pn_2}$ is inside the angle $n_1\widehat{pn}_3$. Then choose a vertex x such

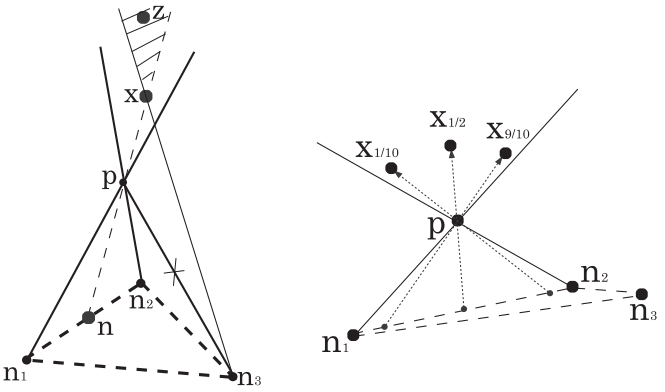

FIG. 5. Left: An uncounterbalanced vertex p with at least three neighbors n_1,n_2,n_3 is counterbalanced by creating bond $\overline{px}$ and deleting bond $\overline{pn_3}$. Likewise, x is counterbalanced by finding z such that x is inside triangle $\triangle zpn_3$, consequently creating bond $\overline{xz}$. Right: An illustration of different positions to choose an appropriate neighbor x for uncounterbalanced vertex p. Values of β are chosen so that most of the space contained in the angle determined by vectors $\overrightarrow{pn_1}$ and $\overrightarrow{pn_2}$ is scanned.

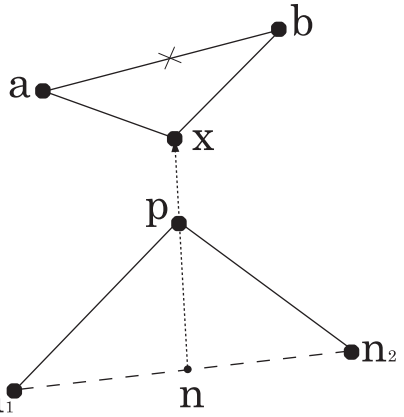

FIG. 6. Uncounterbalanced vertex p is counterbalanced by finding two connected vertices a and b such that the creation of vertex x and bonds $\overline{xp}$,$\overline{xa}$, and $\overline{xb}$ causes x to be counterbalanced. Also, bond $\overline{ab}$ is deleted.

that

$$\overrightarrow{x} = \overrightarrow{n} + \frac{\overrightarrow{np}}{\|\overrightarrow{pn}\|}\alpha, \quad \overrightarrow{n} = \beta\overrightarrow{n_1} + (1-\beta)\overrightarrow{n_2}, \qquad (2)$$

where α is equal to one-half the distance from p to its closest neighbor and $0 < \beta < 1$. To counterbalance p so that it belongs to the triangle $\triangle n_1 n_2 x$, x should be in the angle determined by the vectors $\overrightarrow{n_1p}$ and $\overrightarrow{n_2p}$. By choosing particular values for β, for example $\beta = \frac{1}{10}, \frac{1}{2}, \frac{9}{10}$, most of the region containing the angle is scanned as illustrated in Fig. 5.

New bonds $\overline{xp}$, $\overline{xn_3}$, $\overline{xz}$ are created and the prior bond $\overline{pn_3}$ is deleted. Note that the new bonds cannot cross any of the prior ones. Then, a prior vertex z is chosen such that x is counterbalanced, which means it should be in the striped region in Fig. 5. If the above counterbalance strategy does not work, move p toward n_2 by a fraction of the length $\|\overrightarrow{pn_2}\|$. Once p is moved, the above strategy is tried again. If this particular construction does not work, choose n to be between n_2 and n_3.

(vii) *Counterbalance strategy for a vertex with at least two neighbors:* Assume the situation depicted in Fig. 6, where p is an uncounterbalanced vertex with neighbors n_1 and n_2. In this case, create a new vertex x such that

$$\overrightarrow{x} = \frac{\overrightarrow{np}}{\|\overrightarrow{pn}\|}\alpha, \quad \overrightarrow{n} = \frac{1}{2}(\overrightarrow{n_1} + \overrightarrow{n_2}). \qquad (3)$$

Then find two connected vertices a and b and create bonds $\overline{xp}$, $\overline{xa}$, $\overline{xb}$ and delete the prior bond $\overline{ab}$. This strategy is successful if the new bonds do *not* cross any of the prior ones and if either vertex a or b remains counterbalanced after deleting the bond connecting it. It is important to note that one can apply this strategy for a vertex with more than just two neighbors.

A few comments on the algorithm are in order. (i) The use of $r_{\min}$ and $r_{\max}$ set the local neighborhood from which vertices are connected. It is in this sense that the algorithm is local spatially. (ii) We did not impose counterbalance during the Laman construction because type II Henneberg steps delete bonds so that a counterbalanced vertex at one point during the graph construction may not be counterbalanced at some later point in the construction. Of course, type I Henneberg steps do not delete bonds, but then a sizable fraction of

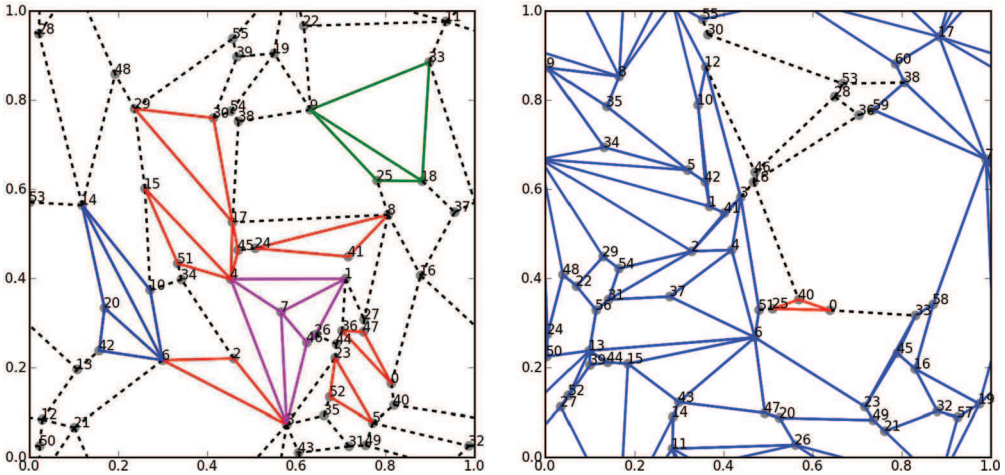

FIG. 7. (Color online) Left: Many small rigid clusters identified via color after the deletion of one bond or contact, namely the bond between vertices 1 and 41 as numbered. The black dashed lines indicate bonds that are not rigid with respect to any other bond. Right: A "macroscopic" rigid cluster along with a few small ones after the deletion of the bond connecting vertices 12 and 30.

uncounterbalanced vertices emerges, approximately 75%, as compared to jamming graphs constructed using the type II Henneberg steps, where approximately 50% of the bonds are counterbalanced automatically. (iii) The algorithm begins with a triangle, which is a $2N-3$ minimally rigid structure. While periodic boundary conditions imply $N_g = 2$, local structures that are the equivalent of the $2N-2$ minimally rigid structure do not include single-bonded triangles. More precisely, for $N = 3$, one connection between two vertices must have a double bond. Since we begin the algorithm with a local structure and build up the graph from there with specific boundary conditions imposed for some fraction of connections that decreases as N increases, we implement $N_g = 3$. The $N_g = 2$ versus $N_g = 3$ for periodic particle packings presumably accounts for why an extra contact is needed for a positive bulk modulus. (iv) The jamming graph is one connected structure, i.e., there are no rattlers. Rattlers are usually removed by hand when studying elastic properties, for example, since they do not contribute to the network. (v) New vertices may be added to the jamming graph to enforce the counterbalance property. We use N to denote the number of vertices before counterbalance is enforced such that the approximate number of final vertices is $\frac{3}{2}N$.

To compare the jamming graph algorithm with other algorithms generating minimally rigid particle packings, such particle-based algorithms range from minimization methods [2] to adaptative network methods [30] to molecular dynamics [31,32] to event-driven molecular dynamics [33]. When using these approaches, the transition point, defined by the packing fraction or the average pressure, can be protocol-dependent [34–36]. Moreover, convergence issues exist [11]. Our algorithm uses purely contact geometry to concretely define the onset of jamming in frictionless spheres. Indeed, there exist algorithms to generate generic disordered minimally rigid graphs via a matching algorithm [37,38], where generic means that the vertex coordinates are not related by any symmetry. These graphs are not planar, nor is local mechanical stability enforced. And finally, there exists a hybrid approach where high-density particle packings are used to generated a disordered hyperstatic graph [39]. Then, bonds are randomly deleted from the graph until, for example, $\langle z \rangle = 4$ is obtained. There is a constraint on the random deletion, however, where a bond is not deleted if the local coordination number of either of the two associated vertices goes below 3, otherwise known as the k-core condition [10]. However, both latter algorithms do not necessarily enforce the geometry of local mechanical stability.

IV. PERTURBING JAMMING GRAPHS

Now that we have an algorithm to construct jamming graphs, we perturb these graphs to determine how the system destabilizes (and restabilizes) mechanically. The destabilization is studied via the identification of rigid clusters. A rigid cluster defines those bonds that are rigid with respect to each other. A rigid cluster is defined on the bonds, as opposed to the vertices, because a vertex can belong to two different rigid clusters, while bonds can be identified with only one rigid cluster. The rigid cluster size s is defined as the total number of bonds belonging to a rigid cluster. We then use the powerful pebble game algorithm [40] to identify rigid clusters via an additional test bond. By construction, the jamming graph is one minimally rigid cluster. We now investigate how the jamming graph destabilizes with the removal of one bond. Note that the size of the rigid clusters is measured in terms of bonds and not vertices.

A. One random bond deletion

The removal of one bond or contact creates exactly one floppy mode such that every bond is no longer rigid with respect to every other bond in the graph. In other words, there must be at least two rigid clusters in the graph. In fact, one can prove that there must be an even number of rigid clusters. So, precisely how many pairs of rigid clusters are there after one bond is randomly deleted? Many microscopic rigid clusters with no rigid cluster of order the system size, or at least one rigid cluster of order the system size coexisting with microscopic sized rigid clusters? We define a rigid cluster

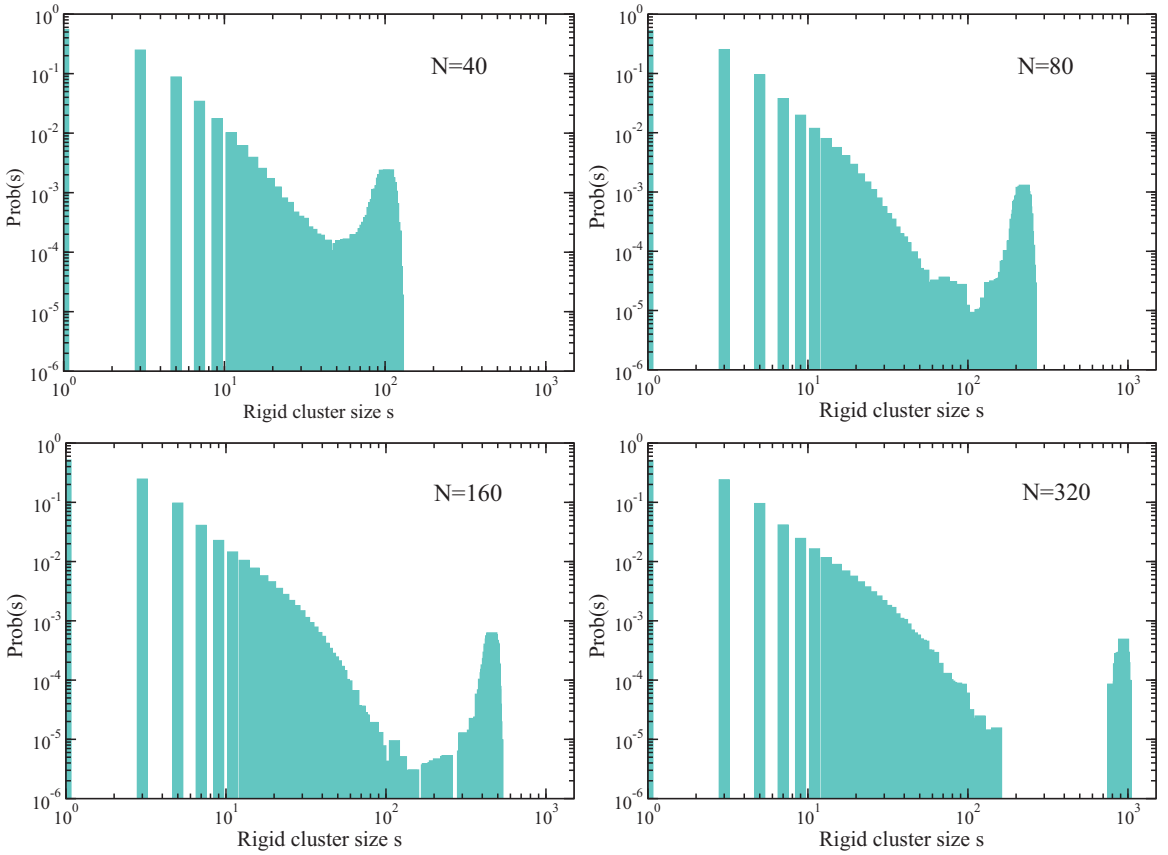

FIG. 8. (Color online) Plot of Prob(s), the probability for a bond to participate in a rigid cluster of size s after one bond is deleted from the jamming graph. The different graphs represent different system sizes.

occupying some large fraction of the bonds in the system and to scale with the system size to be a macroscopic rigid cluster. This macroscopic rigid cluster need not necessarily span the system, though since it scales with the system size, then it is likely too. Microscopic rigid clusters, on the other hand, do not scale with the number of bonds in the system The smallest minimally rigid cluster is a triangle. It turns out that both scenarios are observed. See Fig. 7. And while both scenarios occur, it turns out that the most common scenario is the absence of at least one macroscopic rigid cluster when one bond is deleted.

And while the survival of macroscopic rigid clusters after one bond deletion is apparent in the systems studied, do they persist in the large system limit? Figure 8 depicts the resulting rigid cluster size probability distribution, Prob(s) for $N = 40$, 80, 160, and 320. Note that the rigid cluster size is in terms of bonds such that the rigid cluster sizes can be larger than the initial vertex number N. Indeed, the probability of observing a macroscopic rigid cluster after one bond deletion decreases with increasing system size. To obtain a systematic measurement, we compute the area under the characteristic peak at the macroscopic rigid cluster sizes s, $a^{\#}$. See Fig. 9. While the trend is not clearly power-law nor exponential, the area, $a^{\#}$, is decreasing with N, suggesting that macroscopic rigid clusters after one bond deletion vanish in the infinite system limit. This possibility, while not as likely as the many microscopic rigid clusters scenario, cannot be completely ruled out yet in the infinite system limit, i.e., there is no mathematical proof.

For the sake of argument, consider the graph in Fig. 10 [41]. Removal of the red dashed bond corresponds to each bond not being rigid with respect to any other, or many rigid clusters of size one. However, removal of one of the blue bonds leaves the rest of the rigid structure unchanged (except for

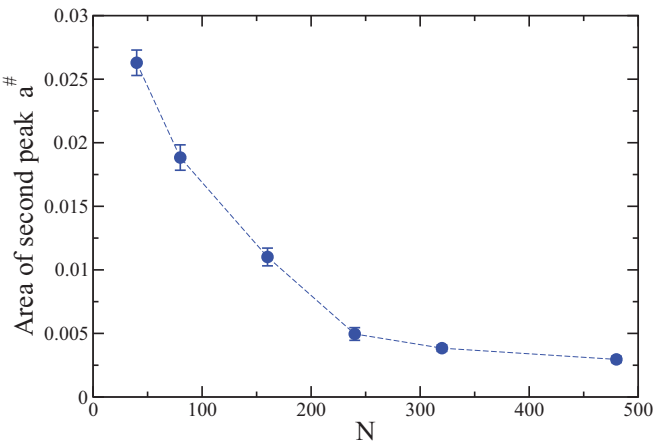

FIG. 9. (Color online) Plot of the peak area for the macroscopic rigid cluster sizes, $a^{\#}$, as a function of N initial vertices. The dashed line is merely a guide for the eye.

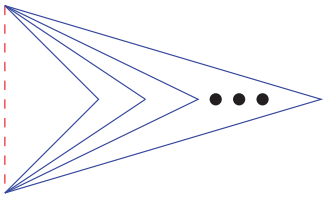

FIG. 10. (Color online) Example graph where removal of the red, dashed line leads to all remaining bonds not rigid with respect to each other. The removal of any one blue line affects only its neighboring blue bond. The rest of the graph is unaffected. The three black circles denote repetition of the blue hinge bonds.

the one neighboring bond that is no longer rigid with respect to any other bond). Depending on the bond that is deleted, either scenario holds in the infinite system limit. And while the specificity of this graph may not be useful for understanding the generic case, extensions of such examples may indeed be.

In the system sizes studied, the two scenarios—(i) many microscopic rigid clusters with no macroscopic rigid cluster and (ii) at least one macroscopic, rigid cluster—can be related to two different floppy modes. In the many microscopic rigid clusters scenario, there is widespread breakup of the system. For bonds between individual rigid clusters, there is zero-energy cost to deforming those bonds such that if they are replaced by springs, as is typically done when determining vibrational modes, these bonds contribute to any zero-energy modes. If these bonds extend across the system, as they do in the case of many microscopic rigid clusters, then the zero-energy mode is an extended one. In contrast, the presence of at least one macroscopic rigid cluster translates to a more localized zero mode since the deforming bonds within the macroscopic rigid cluster will result in some energy cost.

Our finding is presumably related to the recent finding of two kinds of instabilities due to the breaking of contacts in a repulsive, frictionless particle packing at the onset of rigidity [42]. In this work, two particles in contact are pulled apart, i.e., a bond is deleted, and particle rearrangements driven by instabilities are identified. There appear to be two kinds of instabilities—one extended and the other localized. While force information is assumed in this study, our work only uses contact information.

In addition to the decrease in $a^{\#}$ with increasing N, there is another trend in the probability distribution of rigid cluster sizes as the system size increases. A suppression of intermediate cluster sizes starts to emerge, i.e., a gap between the microscopic and macroscopic rigid clusters emerges. There exists an upper bound on the small rigid clusters that does not change with increasing system size. Interestingly, Ref. [11] argued for the absence of intermediate rigid cluster sizes when introducing a surface of cut bonds into the system based on a necessary, but not sufficient, condition for rigidity.

What does a system-size-independent upper bound on the microscopic rigid cluster sizes imply about length scales? Should the macroscopic rigid cluster scenario vanish in the infinite system limit, a diverging length scale emerges in the sense that going from one macroscopic rigid cluster to many microscopic rigid clusters in the infinite system limit corresponds to an infinite length associated with catastrophic breakup of the one minimally rigid cluster.

How does our destabilization result for the jamming graph compare with other minimally rigid graphs, ones where local mechanical stability need *not* be obeyed as with typical rigidity percolation models? To answer this question, we generated minimally rigid graphs using the Henneberg type I move (see Fig. 3), and we did not enforce local mechanical stability (counterbalance) for each vertex. Therefore, we call these graphs type I graphs. We then delete one bond randomly and compute the resulting rigid cluster probability distribution. See Fig. 11. As with jamming graphs, the resulting rigid cluster distribution exhibits two scenarios—one with many microscopic rigid clusters (and no macroscopic rigid cluster) and another less typical scenario with at least one macroscopic rigid cluster—demonstrating a similar trend to the jamming graph case. These results, again, suggest that there are both extended and localized zero-energy modes in a minimally rigid system. However, for the type I graphs, the gap between the macroscopic and microscopic rigid clusters does *not* emerge as clearly as compared to the jamming graph at similar system sizes.

This difference between between the jamming graph and the type I graph could be due to the connectivity of the type I graphs, which is less constrained than the jamming graphs. See Fig. 12. In particular, the fraction of vertices with just two bonds is about 59%. The removal of either bond removes the possibility of that particular vertex participating in any rigid cluster of at least size 3, while for the jamming graph, the removal of a bond does not prevent the neighboring vertex of now two or more neighbors from taking part in another local rigid cluster. In other words, the rigid cluster structures are not as local as in the jamming graph, such that one may have to go to much larger system sizes to observe a gap in the rigid cluster sizes. Interestingly, Goodrich and collaborators [11] did not observe a sudden loss of rigidity for a subsystem size below some length scale for bond-diluted hexagonal lattices—a standard model for two-dimensional rigidity percolation—where vertices of coordination number 2 are allowed. As with type I graphs, it may be that one must go to much larger system sizes to see a gap emerge.

Also, note that the coordination number distribution for the jamming graphs exceeds 6 (Fig. 12). Indeed, the kissing number for a monodisperse disk packing is 6, and it is 12 for a three-dimensional monodisperse sphere packing. In the repulsive soft disk simulations, the size distribution is typically bidisperse (two sizes), where the ratio of the two radii is 1.4 so as to obtain disordered packings [1,2]. However, one also obtains a jamming transition with a polydisperse size distribution. The polydispersity would alter the upper bound of the coordination number distribution, which is nonuniversal, but it would not alter the important universal properties of an average coordination number of 4 and that each particle is enclosed by a triangle by at least three of its neighbors at jamming.

After deleting one bond, let us briefly discuss how the system restabilizes mechanically (or not) with the random addition of one bond. If the added bond is within one rigid cluster, then the bond is redundant and the graph does not restabilize mechanically. However, if the added bond is between two rigid clusters, then it is an independent constraint such that the graph becomes minimally rigid and, therefore,

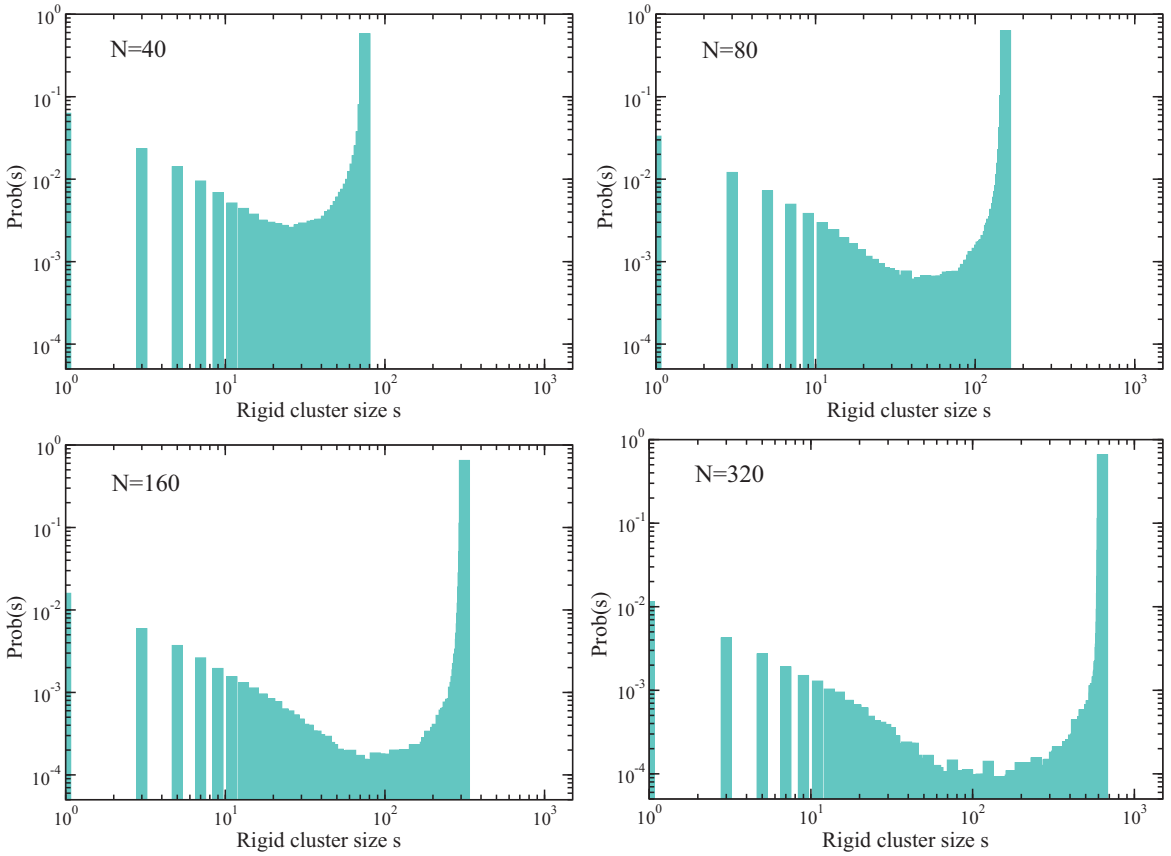

FIG. 11. (Color online) Plot of Prob(s), the probability for a bond to participate in a rigid cluster of size s after one bond is deleted from the minimally rigid graphs generated by Henneberg type I moves only. The different graphs represent different system sizes.

must restabilize mechanically, i.e., there is only one rigid cluster. In terms of a length scale affected by the perturbation, if the destabilized system is made up of many microscopic rigid clusters, the length scale affected by the perturbation is of order the system size, i.e., it is infinite in the infinite system limit, since the system goes from many microscopic rigid clusters to one macroscopic rigid cluster with the addition of one bond.

B. Hyperstatic: Randomly adding and deleting more than one bond

We begin with a jamming graph and randomly add some number of bonds, A. The graph is no longer minimally rigid, i.e., it is now hyperstatic. This action allows us to study systems that are "above" jamming where the macroscopic rigid clusters survive at least one bond deletion. We can then randomly delete (different) bonds from this hyperstatic graph and investigate how the system destabilizes mechanically. We may then be able to identify a length scale that decreases from the system size at jamming to some length scale smaller than the system size as a result of randomly deleting D bonds.

For a concrete example, consider adding eight redundant bonds to a jamming graph with $N = 40$. For 100 000 realizations, the random removal of one bond does not create more than one rigid cluster, i.e., the system is still rigid globally. The random removal of two bonds creates a few small rigid clusters in addition to the macroscopic rigid cluster with a gap in between. See Fig. 13. When three bonds are randomly removed, however, we observe more of a qualitative change in the rigid cluster size distribution. The gap between microscopic rigid clusters and macroscopic rigid clusters closes. The concept of a single system with microscopic rigid clusters distinct from macroscopic rigid clusters no longer makes sense. We are now beginning to observe the extended breakup of the system. The gap size just before the extended breakup sets a size scale, $s^{\#}$. This size scale can be easily converted to a length scale via $s^{\#} \sim (l^{\#})^2$ in two dimensions (assuming compactness).

How does $s^{\#}$ scale with N and with distance to the rigidity transition? We define $\epsilon = \frac{A}{N}$ to describe the distance to the transition. More specifically, since $\langle z \rangle = \frac{2}{N_f}(2N_f - 3 + A)$, with N_f representing the final number of vertices in the graph after counterbalancing, then

$$\langle z \rangle - 4 + \frac{6}{N_f} = \frac{4}{3}\epsilon, \tag{4}$$

where we have included the $1/N_f$ correction in the location of the transition [26,43] and used $\frac{N}{N_f} = \frac{2}{3}$. For fixed ϵ, we observe that $s^{\#}$ increases with increasing N until it begins to reach a plateau that is independent of system size. We also observe that as ϵ decreases, $s^{\#}$ increases, though it will ultimately be cut off by the system size. In other words, $s^{\#}$ is behaving as a size scale near a critical point. See Fig. 14.

To test this hypothesis, we measure $s^{\#}$ as a function of ϵ for several system sizes and attempt finite-size scaling via

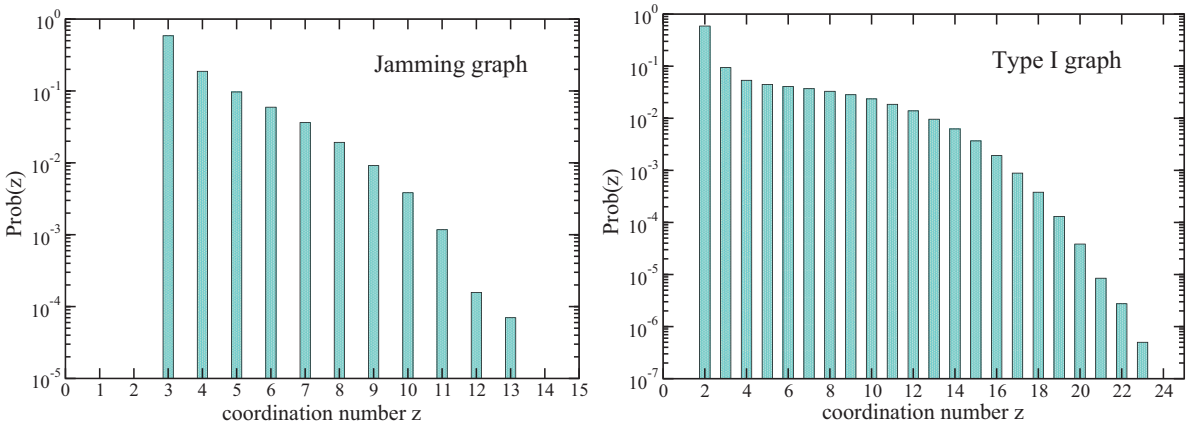

FIG. 12. (Color online) Plot of Prob(z), the probability for a site to have z neighbors, for the jamming graphs (left) and the graphs generated using Henneberg type I moves (right). For both plots, $N = 40$.

the following route. Let $l \sim \epsilon^{-\nu}$, where l is some underlying diverging length scale in the system. If the observed diverging length scale, $l^{\#}$, is due to the underlying diverging length scale, then $l^{\#} \sim \epsilon^{-\rho}$ such that

$$l^{\#} = l^{\rho/\nu} f(l^{1/\nu}\epsilon), \tag{5}$$

with $f(y)$ as some universal scaling function. For the cut-out subsystem analysis with either free or fixed boundary conditions, $\nu = 1$. If we assume this and set $\rho = \nu$, then we do not obtain a good scaling collapse. A more recent discovered diverging length scale, l_c, associated with the localization of phonon modes in floppy networks, results in $\nu = 1/2$ [17,44]. If we again assume $\rho = \nu$, we do not obtain a good scaling collapse. We also tried the two remaining combinations of $\nu = 1$, $\rho = 1/2$ and $\nu = 1/2$, $\rho = 1$ and we did not obtain a good collapse. However, with $\nu = 1/3$ and $\rho = 1/2$, we do obtain a good scaling collapse. See Fig. 14. While these data are suggestive of perhaps a new diverging length scale in the

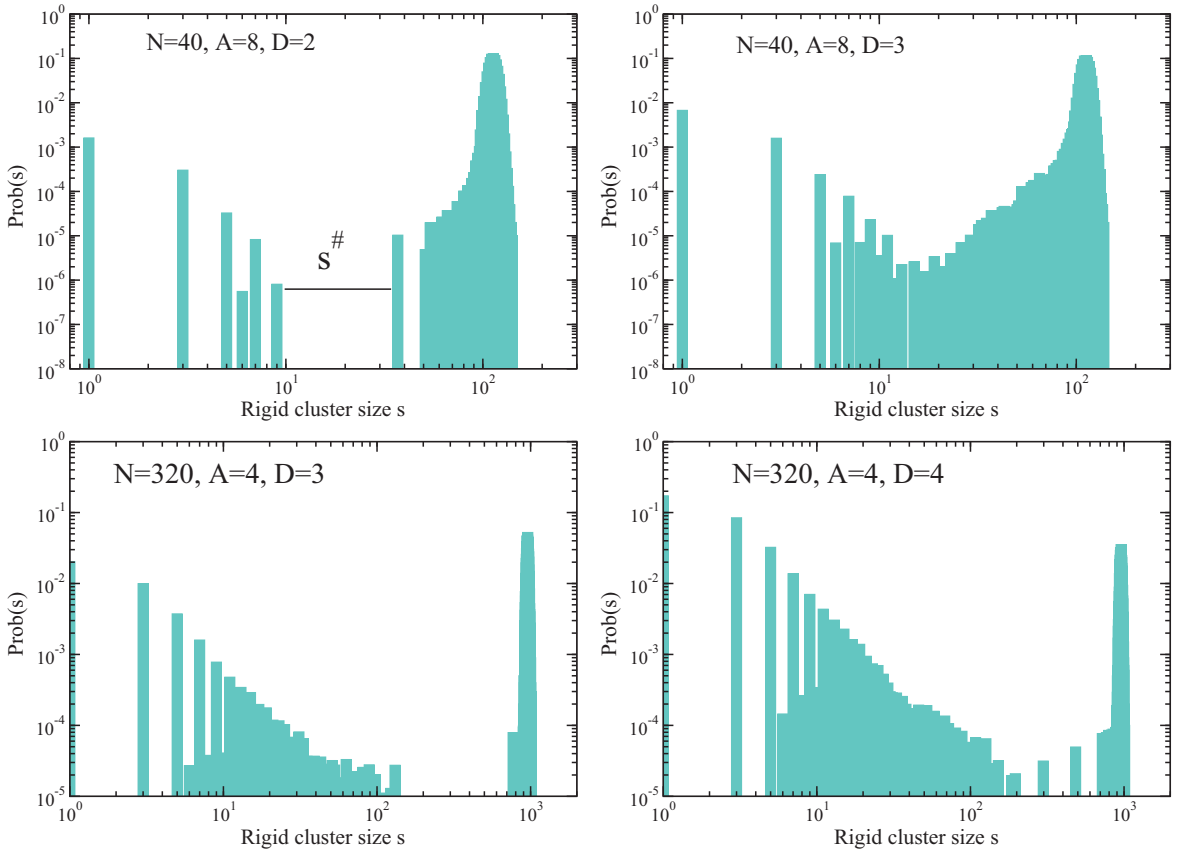

FIG. 13. (Color online) Plot of Prob(s), the probability for a bond to participate in a rigid cluster of size s after A bonds are randomly added to the jamming graph and then D bonds are randomly deleted. Two different system sizes are shown.

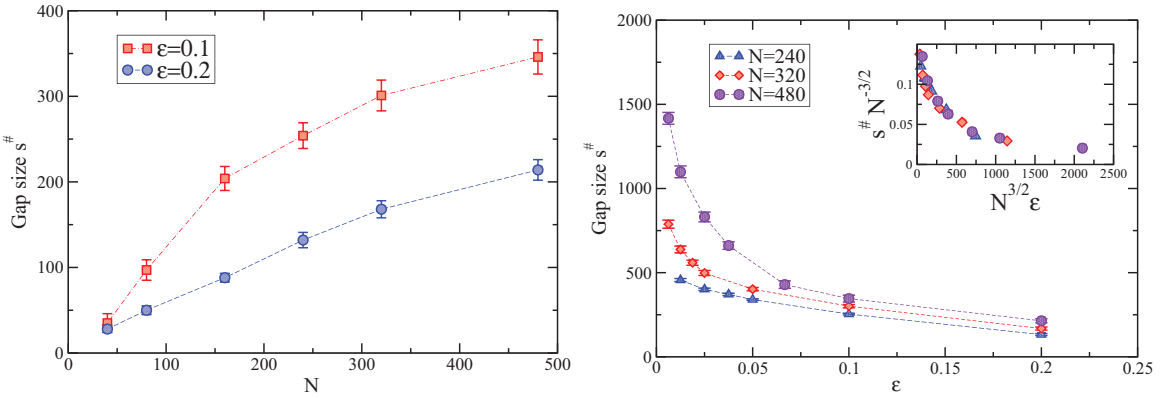

FIG. 14. (Color online) Left: Plot of the gap size $s^{\#}$ as a function of N for fixed $\epsilon = \frac{A}{N}$. Right: Plot of $s^{\#}$ as a function of ϵ for different system sizes. The inset is a finite-scaling scaling collapse obtained with $\nu = \frac{1}{3}$ and $\rho = \frac{1}{2}$. All dashed lines are guides for the eye.

system associated with point perturbations via $\nu = 1/3$, this possibility may be ruled out by the study of larger system sizes.

It is interesting to note that mean-field correlation length exponents of $1/4$, $1/2$, and 1 exist in disordered systems [8–10,17,44], while a correlation length exponent of $1/3$ is presumably less common. Incidentally, while $\nu = 1/4$ (and $\rho = 1/2$) is not as good a collapse as with $\nu = 1/3$, it cannot be ruled out at this stage. However, we can conclude that $\nu = 1, 1/2$ and/or $\rho = 1, 1/2$ does not lead to sufficient collapse for at least the system sizes we study.

V. DISCUSSION

We have presented an algorithm for the spatially local construction of jamming graphs. Jamming graphs represent the contact geometry of frictionless, repulsive soft disks in two dimensions at the onset of mechanical rigidity. In other words, they contain both the property of local mechanical stability and the necessary and sufficient condition for minimal rigidity via the Henneberg construction. Since the bonds represent contacts between particles or vertices, the jamming graph is planar. Varying the construction of these (and related) graphs allows us to turn on (off) different properties of particle packings at (near) the onset of rigidity in a controlled way to ultimately form a more concrete and comprehensive picture of jamming.

Our construction of jamming graphs begs at least three immediate extensions of study. For the first extension, if one associates a disk with each vertex and each bond dictates the contact between two disks, then we can potentially analyze the question of whether there exists a unique packing fraction at the onset of rigidity in the infinite system limit [2,34,45–47]. Indeed, there have been a number of different definitions of the onset of jamming ranging from the random closed packing (RCP) point [2,48] to a maximally jammed state [45] to a jamming line [46,47]. To address this issue, we can create a physical realization of disks from a jamming graph using the circle packing theorem [49]. The circle packing theorem states that for every connected simple planar graph G, there exists a circle packing in the plane whose intersection graph is isomorphic to G. There are more strict conditions for uniqueness as such, and these will be explored. Note that to more readily associate a jamming graph with a disk packing, we will allow for a polydisperse size distribution of disks. While we can immediately explore this issue in two dimensions where Laman's theorem is exact and the circle packing theorem holds, it would be interesting to extend the jamming graph to three dimensions and higher. It turns out that the three-dimensional version of Laman's theorem for some networks is essentially exact [50]. Higher-dimensional extensions of the circle packing theorem would indeed be more challenging.

As for the second immediate extension, with jamming graphs we can search for an interplay between global mechanical stability and local mechanical stability since we can easily turn off or on local mechanical stability. This on-off switch allows us to compare the mechanics of fixed connectivity networks from rigidity percolation [20,21] with repulsive particle packings [14,17,39,51]. While local mechanical stability may not play as much of a role at the transition (other than suppressing fluctuations [9]), it will certainly play a role in particle rearrangements above jamming, where local mechanical stability is also required. For instance, if particle chains form as a result of some perturbation, the chain should buckle so that particles having two contacts will ultimately have at least three contacts with the appropriate geometry. Such particle rearrangements above jamming can also be studied using jamming graphs with the removal and addition of bonds. For instance, if the breaking of a contact results in a vertex not being counterbalanced, with some added force information [42,52–54], a sequence of moves can be generated to regain the local mechanical stability while ensuring that the graph remain hyperstatic.

For the third immediate extension, local rules governing a system may lead to a field theory, should one exist. And while there is not necessarily a consensus on a field theory for jamming [55,56], our spatially local construction of the jamming graph may provide insight for building a modified field theory for a system with both local and global constraints. Such a framework may accelerate the quest to determine how to classify the various constraints in terms of potentially different universality classes. For instance, enforcing only the local k-core constraint leads to one type of phase transition, while the counterbalance constraint leads to another [10,57].

And while such attempts are not currently appreciated in the field, a classification system based on constraints will ultimately emerge.

For instance, the notion of constraints changes when one deviates from frictionless, repulsive soft disks. Ellipsoidal particle packings may or may not be isostatic at the onset of rigidity, depending on which degrees of freedom can be accessed [58,59]. It turns out that one can also extend Laman's theorem in two dimensions to systems with other degrees of freedom [28] and, correspondingly, extend the Henneberg construction. Such an extension of the jamming graph may, therefore, prove useful for understanding the onset of rigidity for nonspherical particles. As for frictional systems, while the history of the contact information may be difficult to incorporate into an equivalent jamming graph, one can extend the pebble game [to a (3,3) pebble game] to map out the rigid clusters of frictional packings to compare with frictionless packings [60]. These endeavors (and others) will help form a concrete framework for the onset of rigidity in disordered systems.

After constructing these jamming graphs, the deletion of one bond allows us to study how the system destabilizes. In the system sizes studied, there exist two scenarios, one in which the removal of the bond leads to catastrophic collapse of the single rigid cluster with many microscopic rigid clusters (an extended zero-energy mode), and the other in which at least one macroscopic rigid cluster survives (a localized zero-energy mode). As the system size increases, the probability of the localized zero-energy mode decreases. It would be interesting to prove whether this probability vanishes in the infinite system limit. Particularly in two dimensions, there is a wealth of mathematical literature on minimal rigidity to potentially go beyond heuristic arguments and numerics.

As opposed to uncovering a diverging length scale in surface versus bulk effects [8,9,11,12,14], we have potentially uncovered a new diverging length scale in the rigid phase in response to random bond deletion. With a correlation length exponent close to $1/3$, it appears that this new length scale is not related to the introduction of a force monopole in the particle packings [16]. However, once forces are introduced, and/or the contact geometry is allowed to rearrange as the system responds to the point perturbation, then one should presumably obtain the prior result. Again, the ability to build upon the jamming graph by incorporating further detail bit-by-bit will allow us to identify the properties ultimately dictating a particular behavior or response.

ACKNOWLEDGMENTS

The authors acknowledge helpful discussions with Silke Henkes, Xu Ma, and Brigitte Servatius. J.M.S. acknowledges funding from NSF-DMR-CAREER-0607454 and the Aspen Center of Physics, where part of this work was completed.

[1] C. S. O'Hern, S. A. Langer, A. J. Liu, and S. R. Nagel, Phys. Rev. Lett. **88**, 075507 (2002).
[2] C. S. O'Hern, L. E. Silbert, A. J. Liu, and S. R. Nagel, Phys. Rev. E **68**, 011306 (2003).
[3] A. J. Liu, M. Wyart, W. van Saarloos, and S. R. Nagel, in *Dynamical Heterogeneities in Glasses, Colloids and Granular Media*, edited by L. Berthier, G. Biroli, J.-P. Bouchaud, L. Cipelletti and W. van Saarloos (Oxford University Press, Oxford, 2011).
[4] M. van Hecke, J. Phys.: Condens. Matter **22**, 033101 (2010).
[5] A. J. Liu and S. R. Nagel, Annu. Rev. Condens. Matter Phys. **1**, 347 (2010).
[6] S. Alexander, Phys. Rep. **296**, 65 (1998).
[7] D. Stauffer and A. Aharony, *Introduction to Percolation Theory*, 2nd ed. (Taylor and Francis, New York, 1992).
[8] M. Wyart, S. R. Nagel, and T. A. Witten, Europhys. Lett. **72**, 486 (2005).
[9] M. Wyart, L. E. Silbert, S. R. Nagel, and T. A. Witten, Phys. Rev. E **72**, 051306 (2005).
[10] J. M. Schwarz, A. J. Liu, and L. Q. Chayes, Europhys. Lett. **73**, 560 (2006).
[11] C. P. Goodrich, W. G. Ellenbroek, and A. J. Liu, arXiv:1301.6981.
[12] M. Mailman and B. Chakraborty, J. Stat. Mech. (2011) L07002.
[13] M. Mailman and B. Chakraborty, J. Stat. Mech. (2012) P05001.
[14] B. P. Tighe, Phys. Rev. Lett. **109**, 168303 (2012).
[15] W. G. Ellenbroek, E. Somfai, M. van Hecke, and W. van Saarloos, Phys. Rev. Lett. **97**, 258001 (2006).
[16] W. G. Ellenbroek, M. van Hecke, and W. van Saarloos, Phys. Rev. E **80**, 061307 (2009).
[17] G. During, E. Lerner, and M. Wyart, Soft Matter **9**, 146 (2012).
[18] H.-K. Janssen and U. C. Tauber, Ann. Phys. **315**, 147 (2005).
[19] M. F. Thorpe, J. Non-Cryst. Solids **57**, 355 (1983).
[20] S. Feng and P. N. Sen, Phys. Rev. Lett. **52**, 216 (1984).
[21] S. Feng, M. F. Thorpe, and E. Garboczi, Phys. Rev. B **31**, 276 (1985).
[22] D. J. Jacobs and M. F. Thorpe, Phys. Rev. Lett. **75**, 4051 (1995).
[23] D. J. Jacobs and M. F. Thorpe, Phys. Rev. E **53**, 3682 (1996).
[24] C. Moukarzel and P. M. Duxbury, Phys. Rev. Lett. **75**, 4055 (1995).
[25] J. C. Maxwell, Philos. Mag. **27**, 294 (1864).
[26] G. Laman, J. Engrg. Math. **4**, 331 (1970).
[27] L. Henneberg, Die graphische Statik der starren Systeme, Leipzig (1911) (unpublished).
[28] I. Streinu and L. Theran, Eur. J. Comb. **30**, 1944 (2009).
[29] G. Berg, W. Julian, R. Mines, and F. Richman, Rocky Mount. J. Math. **5**, 225 (1975).
[30] A. V. Tkachenko and T. A. Witten, Phys. Rev. E **60**, 687 (1999).
[31] L. E. Silbert, D. Ertaş, G. S. Grest, T. C. Halsey, and D. Levine, Phys. Rev. E **65**, 031304 (2002).
[32] P. Olsson and S. Teitel, Phys. Rev. Lett. **99**, 178001 (2007).
[33] A. Donev, F. H. Stillinger, and S. Torquato, J. Comp. Phys. **225**, 509 (2007).
[34] P. Chaudhuri, L. Berthier, and S. Sastry, Phys. Rev. Lett. **104**, 165701 (2010).

[35] D. Vågberg, D. Valdez-Balderas, M. A. Moore, P. Olsson, and S. Teitel, Phys. Rev. E **83**, 030303(R) (2011).
[36] S. Dagois-Bohy, B. P. Tighe, J. Simon, S. Henkes, and M. van Hecke, Phys. Rev. Lett. **109**, 095703 (2012).
[37] C. Moukarzel, J. Phys. A **29**, 8079 (1996).
[38] C. Moukarzel, Europhys. Lett. **97**, 36008 (2012).
[39] W. G. Ellenbroek, Z. Zeravcic, W. van Saarloos, and M. van Hecke, Europhys. Lett. **87**, 34004 (2009).
[40] D. J. Jacobs and B. Hendrickson, J. Comp. Phys. **137**, 346 (1997).
[41] This example was pointed out to us by Brigitte Servatius.
[42] E. Lerner, G. Düring, and M. Wyart, arXiv:1302.3990.
[43] C. P. Goodrich, A. J. Liu, and S. R. Nagel, Phys. Rev. Lett. **109**, 095704 (2012).
[44] M. Wyart, Europhys. Lett. **89**, 64001 (2010).
[45] S. Torquato, T. M. Truskett, and P. G. Debenedetti, Phys. Rev. Lett. **84**, 2064 (2000).
[46] G. Parisi and F. Zamponi, Rev. Mod. Phys. **82**, 789 (2010).
[47] P. Charbonneau, E. I. Corwin, G. Parisi, and F. Zamponi, Phys. Rev. Lett. **109**, 205501 (2012).
[48] J. D. Bernal and J. Mason, Nature (London) **188**, 910 (1960).
[49] K. Stephenson, *Introduction to Circle Packing* (Cambridge University Press, New York, 2005).
[50] M. V. Chubynsky and M. F. Thorpe, Phys. Rev. E **76**, 041135 (2007).
[51] B. Tighe, arXiv:1305.5574.
[52] A. R. T. van Eerd, W. G. Ellenbroek, M. van Hecke, J. H. Snoeijer, and T. J. H. Vlugt, Phys. Rev. E **75**, 060302(R) (2007).
[53] B. P. Tighe, A. R. T. van Eerd, and T. J. H. Vlugt, Phys. Rev. Lett. **100**, 238001 (2008).
[54] S.-L.-Y. Xu, X. Illa, and J. M. Schwarz, arXiv:1008.4568.
[55] S. Henkes and B. Chakraborty, Phys. Rev. Lett. **95**, 198002 (2005).
[56] H. Jacquin, L. Berthier, and F. Zamponi, Phys. Rev. Lett. **106**, 135702 (2011).
[57] M. Jeng and J. M. Schwarz, Phys. Rev. E **81**, 011134 (2010).
[58] M. Mailman, C. F. Schreck, C. S. O'Hern, and B. Chakraborty, Phys. Rev. Lett. **102**, 255501 (2009).
[59] Z. Zeravcic, N. Xu, A. J. Liu, and S. R. Nagel, Europhys. Lett. **87**, 26001 (2009).
[60] S. Henkes, Y. Fily, D. Quint, and J. M. Schwarz (unpublished).